East African Scholars Multidisciplinary Bulletin
Abbreviated Key Title: East African Scholars Multidiscip Bull
ISSN 2617-4413 (Print) | ISSN 2617-717X (Online)
Published By East African Scholars Publisher, Kenya
Volume-7 | Issue-5 | Jul-2024 | DOI: 10.36349/easjmb.2024.v07i05.001

OPEN ACCESS

Original Research Article

Photocatalytic activity of Nb2O5-α-Fe2O3 Nanocomposites Synthesized by Sol-gel Method

M.J. Pawar[1*], A.D. Khajone[1], M.D. Gaonar[1]

[1]Laboratory of Materials, Synthesis, department of Chemistry, Smt. Narsamma ACS College, Kiran Nagar, Amravati M.S. Bharat 444606

Article History
Received: 07.12.2023
Accepted: 18.01.2024
Published: 13.07.2024

Journal homepage:
https://www.easpublisher.com

Quick Response Code

Abstract: In this investigation, Nb_2O_5-α-Fe_2O_3 nanocomposites were synthesized by modified sol-gel method. The obtained materials were characterized by different techniques such as powder X-ray diffraction (XRD), field-emission scanning electron microscopy (FESEM), Brunauer-Emmett-Teller (BET), UV-vis diffuse reflectance (UV-vis spectroscopy). The catalyst was found to have a particle size in the region of 20-42 nm with a high surface area. The effects of the catalyst dose, the pH value, UV power, addition of H_2O_2 and scavenger on the photocatalytic efficiency were investigated. This study presents a strategy to eliminate highly toxic and persistent dyes such as DB 199 dye. It was observed that the nanocomposites showed maximum response with more than 80% degradation of DB 199 dye in 100 min.

Keywords: Nb_2O_5: α-Fe_2O_3: Nanocomposites: Photocatalysis: DB 199 dye.

1. INTRODUCTION

Owing to promising potential applications in battery cathode material, non-linear optics, Ionics, nanowires, photocatalysts and sensors, nanocomposites are of great interest in materials science [1]. For the past few decades, there has been considerable research in nanocomposites through the change in matrix phase and other geometrical variations helpful in applications enhancement of the materials. Hematite (α-Fe_2O_3), as a promising photocatalyst, has been widely investigated in photocatalytic degradation of organic contaminants [2]. It is the most stable state of iron oxides in ambient conditions and has the ability of efficient photodegradation and is able to harvest visible light up to 600 nm [3, 4]. Other salient features of hematite include its excellent stability, less toxicity, lower cost, inert behaviour and antiferromagnetic properties, also appeal its wide applications [5, 6]. The unfavourable defects of hematite structure, such as poor charge–transfer properties and faster recombination of charged species, are urged to be diminished. It was suggested that these structural and photochemical deficits can be possibly improved in multiple ways including morphological control, surface modification, synthesis of heterostructures and composites and/or doping with some other materials [7, 8]. Various previous studies indicated that coupling semiconductor metal oxides with hematite induces more active sites at the interface, which is favourable for photocatalysis [9-11]. Niobium pentoxide (Nb_2O_5), a typically nontoxic metal oxide, is eco-friendly and exhibits strong oxidation ability, and has attracted considerable attention from researchers. The applications of Nb_2O_5 based photocatalysts are reported in the photodegradation of plastics, reduction of CO_2, photocatalytic hydrogen evolution, and organic synthesis [12-16].

Dyes are widely used in many industries, such as the textile, rubber and cosmetics industries [17-20]. More than 10,000 types of dyes are suitable for industrial use and more than thousands of tons are produced in the world during the year [21]. Most of these dyes in nature not only create an unpleasant appearance but also weaken the penetration of light, reduce photosynthetic activity and inhibit biological growth. In addition, most of these dyes are toxic and carcinogenic. The aim of the present investigation was to synthesize Nb_2O_5-Fe_2O_3 nanocomposites by sol-gel method and study the photocatalytic degradation of Direct Blue 199 dye under the influence of UV and visible. The structure and surface physicochemical characterization of the synthesized materials were analyzed by X-ray diffraction (XRD) analysis, field-emission scanning electron microscopy (FESEM) and UV-visible spectroscopy. The

***Corresponding Author:** M.J. Pawar
Laboratory of Materials, Synthesis, department of Chemistry, Smt. Narsamma ACS College, Kiran Nagar, Amravati M.S. Bharat 444606

effects of pH of the solution, photocatalyst dosage, effect of UV power, effect of H_2O_2 addition on the degradation efficiency were investigated.

2. EXPERIMENTAL

2.1 Synthesis of α-Fe_2O_3 nanoparticles

The method of synthesis of is mentioned in *Chapter IV* of the thesis. For the synthesis of α-Fe_2O_3 nanoparticles calculated quantity of $FeN_3O_9.9H_2O$ was mixed with 40 cc ethylene glycol and the mixture was stirred at 60˚C for 2 h. An aqueous solution of NH_3 was added under continuous stirring to give the corresponding pH in each synthesis. The reaction mixture was maintained at room temperature until a gel was formed; once the colloid was observed, it was kept for aging for 18 h which was dried in the oven at 80°C and then calcined in muffle furnace at 450°C for 4 h.

2.2 Synthesis of Nb_2O_5-α-Fe_2O_3 nanocomposites

For the synthesis of Nb_2O_5-α-Fe_2O_3 nanocomposites by sol-gel method, in a conical flask, 40 cc of niobium ethoxide was mixed with 90 cc of isopropanol and the solution was homogenized. In another flask, 15 cc of deionized water was mixed with the 25 cc ethanol-isopropanol (1:1) mixture and homogenized. Content of the second flask was added to the first flask. In order to reach the acidic pH of 4, hydrochloric acid was added dropwise to the mixture. Then calculated amount of α-Fe_2O_3 synthesized in the previous step was combined with the above solution and the mixture was placed on a magnetic stirrer for 2 hours. The obtained mass was then allowed to age for 18 h to obtained viscous gel. The resulting gel was dried in the oven at 100°C for 2 hours and obtained dry gel was heat-treated at 450°C and 500°C for 4 hours. The two nanocomposites obtained by heat treatment at 450°C and 500°C were referred as NF45 and NF50 respectively.

2.3 Characterization

As-synthesized samples were examined by X-ray diffraction (XRD) measurements on a Shimadzu X-ray diffractometer, equipped with Cu-Kα radiation source (λ = 0.154056 nm) at a scan rate of 5 min^{-1}. Bragg angle 2θ was ranged from 10 to 70°. Scanning electron micrographs were observed on a Zeiss Sigma Scanning Electron Microscope (SEM) operated at an acceleration voltage of 20 kV. The nitrogen adsorption/desorption isotherms at 77.35K were collected on an AUTOSORB iQ-MP instrument after heating the samples at 150°C for 2 h. The surface areas were estimated using the Brunauer-Emmett-Teller (BET) method.

2.4 Study of Photocatalytic Activity

The experimental set up used for photocatalytic degradation performance of Nb_2O_5-α-Fe_2O_3 nanocomposites is expressed in detail in *Chapter IV*. The photocatalytic test was carried out using a UV-photo reactor. Blue light fluorescent bulbs were positioned at the axis of the reactor to supply UV illumination. The reaction suspension was irradiated by UV light at a power of 18 W. In a typical photocatalytic degradation reaction, 10-40 mg/L of the catalyst powder was dispersed solution containing 50-200 ppm Direct Blue 199 dye and stirred for 1 h. Before starting the photocatalytic reaction, the reactor was kept in the dark and stirred for 30 min to ensure the adsorption/desorption equilibrium. During this time, dye molecules were adsorbed on the catalyst surface. Subsequently, the reactor was exposed to UV-light. At the interval of every 30 min, 5 mL aliquots were taken from the reaction mixture. The reaction mixture was then centrifuged, and the absorbance of the supernatant was measured by UV–Vis spectroscopy at the maximum absorption wavelength of the Direct Blue 199 dye (λ_{max} = 662 nm). The percentage of degradation efficiency was estimated by Equation (I);

$$\text{Degradation (\%)} = \frac{C_o - C}{C_o} \times 100 \qquad (1)$$

where C_o and C denote the absorbance initially before exposure to UV-light and after exposure time t, respectively.

3. RESULT AND DISCUSSION

3.1 X-ray diffraction

The purity and crystallinity of the as-prepared powder samples are measured by X-ray diffraction technique. XRD results reveal that the prepared α-Fe_2O_3 nanoparticles have a rhombohedral structure with the diffraction characteristic peaks are indexed as (012), (104), (110), (113), (024), (116), (018), (214), (300), and (220) planes corresponding to pure α-Fe_2O_3. The data were well corroborated with the literature data JCPDS card No. 84-0311 [22]. The presence of sharp, narrow, and highly intense peaks in the spectrum indicates the crystalline nature and purity of the synthesized α-Fe_2O_3 sample. The average crystallite size calculated from the most intense peaks using the Scherrer formula (Equation (II)). The average crystal size was found to be 27.4 nm.

$$D = \frac{0.9\lambda}{\beta cos\theta} \qquad (2)$$

Where, D refers to the average crystallite size, λ is the wavelength of the *Cu Kα* X-ray radiation = 0.15406 nm, β refer to the full width at half maximum intensity of the peaks and θ and the Bragg angle, both measured in radians, respectively. XRD pattern of Nb_2O_5-α-Fe_2O_3 nanocomposites showed that the peaks observed belong to the α-Fe_2O_3 phases only. The reason for the absence of peaks related to Nb_2O_5 could be its low percentage in the nanocomposite and relatively lower calcination temperature employed in our experiment. From Figure 1, it can be seen that, at 450°C, intensity of peaks is smaller and increases strongly at 550°C.

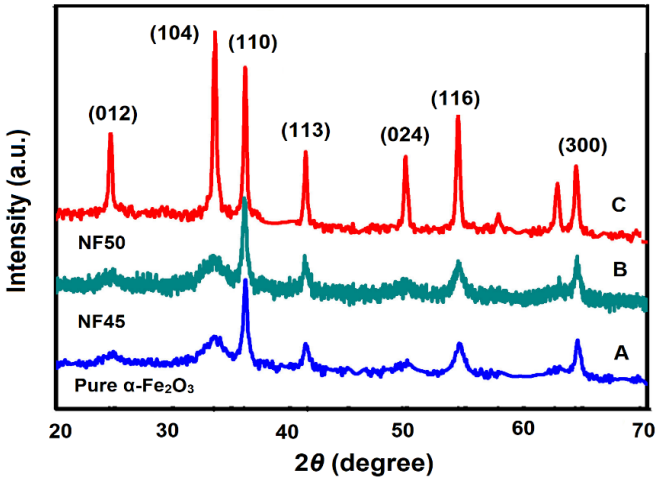

Figure 1 XRD pattern of pure α-Fe_2O_3 nanoparticles and Nb_2O_5-α-Fe_2O_3 nanocomposites

3.2 Brunauer Emmet Teller (BET) surface area analysis

Specific surface area of as-prepared samples of nanocomposites was assessed using Brunauer Emmet Teller (BET) plot with relative pressure (p/p^o) ranging from 0.01 to 0.20. The sample calcined at the temperature 450°C has a specific surface area (NF45) of 207.35 m^2gm^{-1} as compared to the sample calcined at higher temperature of 500°C whose specific surface area (NF50) was 292.54 m^2gm^{-1}. It was concluded that the heat-treatment temperature has large effect on the surface area modification of Nb_2O_5-α-Fe_2O_3 nanocomposites.

3.3 UV-visible analysis

The UV-visible absorption spectrum of α-Fe_2O_3 and sample NF45 presented in Figure 2 shows three absorption bands at around 357, 539 and 672 nm. The absorption band present in the region of 400-600 nm can be assigned to d-d transition of Fe^{3+} as well as the pair excitations, 6A1 + 6A1 → 4T2 (4G) + 4T2 (4G) of two adjacent Fe^{3+} cations (6A1 and 4T2 (4G)), referred to as the ground state and first excited state configuration of high spin Fe^{3+}, respectively. Also, the band at 350 nm is mainly results from the ligand to metal charge- transfer transitions and partly from the contributions of the Fe^{3+} ligand-field transition 6A1 → 4T 2 (4D) [23]. The estimated band gap of the sample is found to be 2.03 eV for sample NF45 which is in good agreement with a band gap value of α-Fe_2O_3 [24]. The absorption edge in sample NF45 is indicative of the uniform particle morphology and size with fairly good crystallinity.

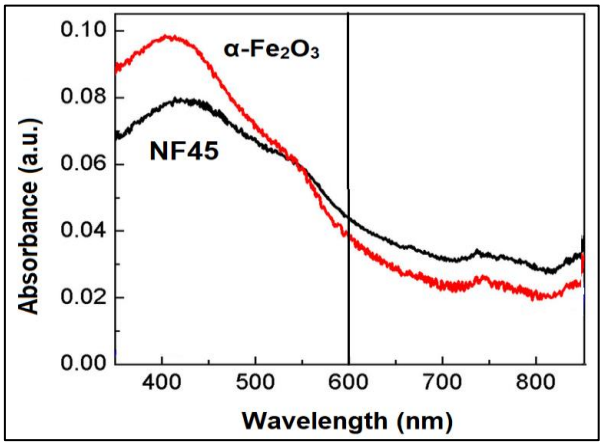

Figure 2. UV-visible absorption spectrum of pure and NF45 samples

3.4 SEM analysis

Figure 3 shows the top view of FESEM images of as-prepared samples. A large number of nanoparticles are clearly observed with diameters in range of 20 -70 nm. In the high magnification FESEM image shown in the Figure 3, the particles can be observed to be composed of many rough surfaces and having non-uniform shapes polyhedral shape. Thus, the nanoparticles obtained at two different temperatures, 450°C and 500°C are clearly distinguishable in shape and surface morphology. It is suggested that the operating temperature of heat treatment significantly affect the shape and surface morphology of the nanoparticles.

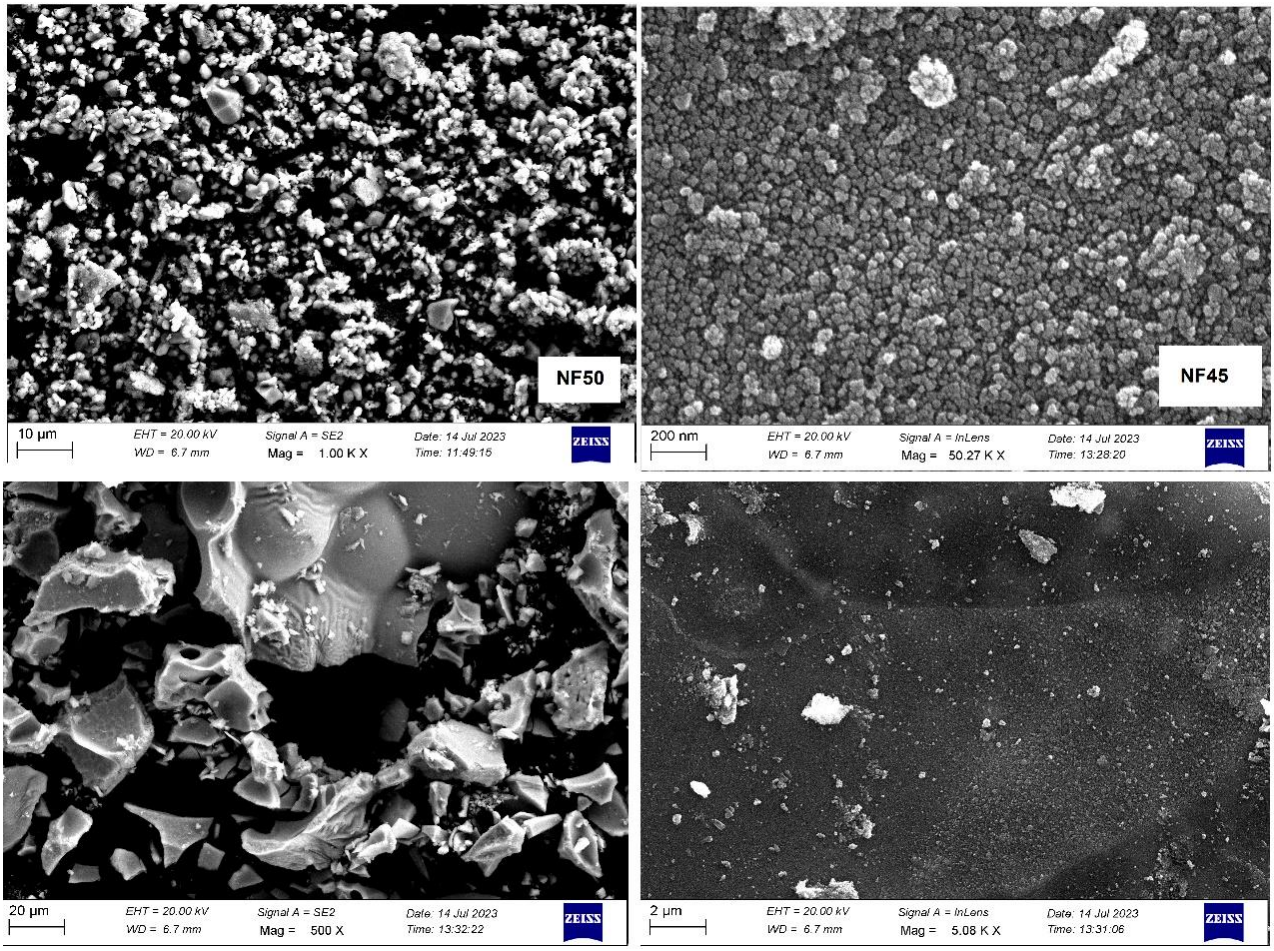

Figure 3. SEM micrographs of α-Fe_2O_3, NF45 and NF50 samples

3.5 Photodegradation of direct blue 199 (DB) dye

3.5.1 Dark Reactions

The adsorption of dye was equilibrated onto the surface of as-prepared nanocomposites (figures are not shown) was studied initially. It was observed that regardless of the initial concentrations of the parent compounds, the steady state adsorption of dye was obtained after 50 min. The process was continued for 4 h and no significant reduction was observed.

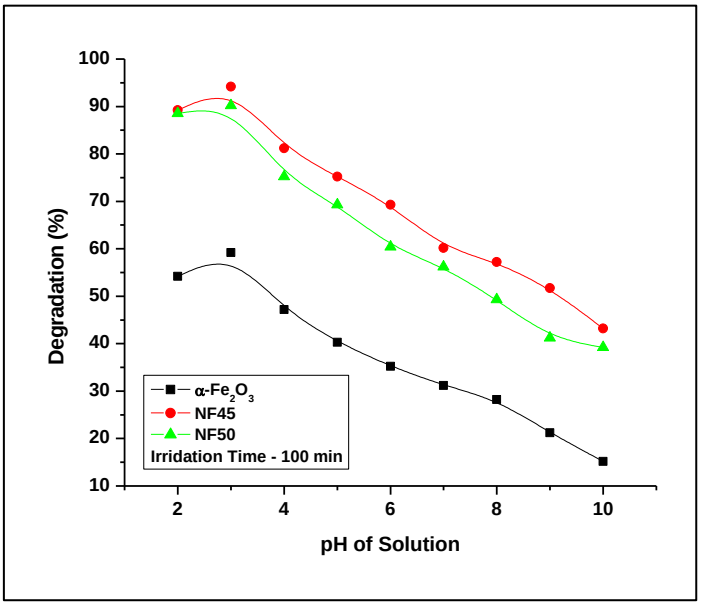

Figure 4. Effect of pH on photodegradation of DB 199 dye (100 ppm)

3.5.2 Effect of pH

The pH is an important parameter in the photocatalytic reactions taking place on the particulate surfaces as it dictates the surface charge properties of the photocatalyst. As reported earlier, the pH value has an influence on the kinetic of degradation of some organic compounds in photocatalytic processes [26-28]. In the present investigation, the degradation of DB dye (100 ppm) was studied at different pH values in the range 2 – 10 and the results are presented in Figure 4. The experimental results revealed that higher degradation of dye was found to be in strong acidic medium. The maximum degradation was observed at pH 3. This may be attributed to the electrostatic interactions between the positive catalyst surface and dye anions leading to strong adsorption of the latter on the metal oxide support. Moreover, the positive holes are considered as the major oxidation species formed at low pH which react with hydroxide ions forming hydroxyl radicals, thus the efficiency of process is enhanced. At increased pH, there is a columbic repulsion between negatively charged surface of catalyst and the hydroxide anions which prevent the formation of OH° and decrease the photocatalytic degradation [29].

3.5.3 Effect of catalyst loading

The effect of catalyst loading on the degradation of DB 199 dye was investigated using the varying concentration of as-prepared materials, keeping the other parameters identical. The results of this study are shown in Figure 5. One can see from Figure 5, that the maximum 99% degradation efficiency of DB 199 dye was observed for 20 mg/L of sample NF45 under UV-light within 100 min. A series of experiments were carried out by varying the catalyst amount from 10-40 mg/L in the aqueous solution of DB 199 dye. It can be seen that, initially the degradation efficiency increases with increase in amount of catalyst. With the catalyst dose 20 mg/L, the efficiency of dye degradation was found to be high and then efficiency decreased as the catalyst amount increased. This observation can be explained in terms of the number of active sites available for photocatalytic reactions. It was observed that large amount of catalyst may result in agglomeration of the catalyst molecules resulting in the decrease in the number of active sites [30, 31]. Another reason for decreased degradation efficiency can be attributed to increase in the turbidity of suspension due to excess of photocatalyst. This leads into the scattering of light resulting in the inhibition of photon absorption by the photocatalyst and hence the degradation efficiency.

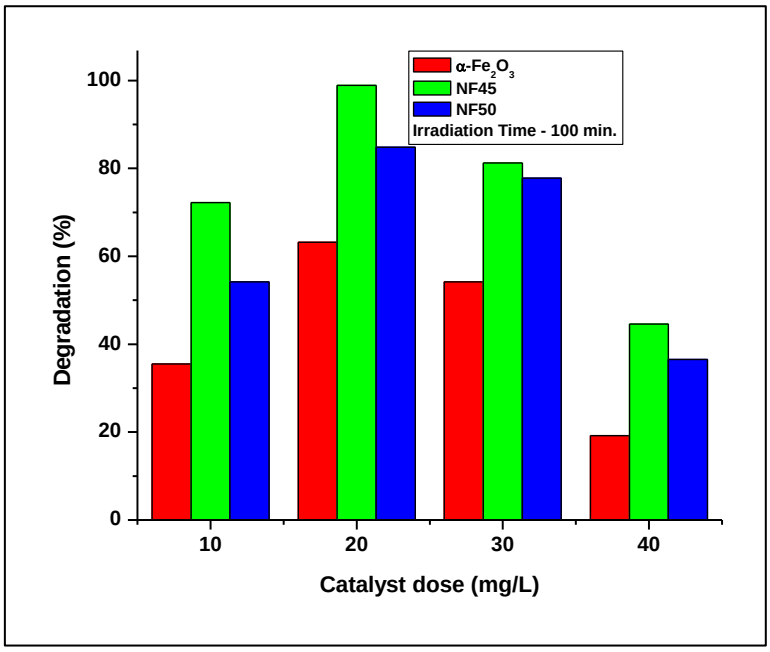

Figure 5. Effect of catalyst dose on photodegradation of DB 199 dye

3.5.4 Effect of UV power

In photodegradation process, the production of electron and hole pairs is governed by the intensity of the illuminated light. The light intensity plays an important role in the photocatalytic degradation reaction as it has a direct effect on the formation of the active hydroxyl radicals [30]. This is an essential step in the formation of the active radicals for the photocatalytic degradation process. Thus, the higher the light intensity, more the transfer of the electrons from the valence band to the conduction band of photocatalyst, consequently the more generation of the hydroxyl or oxygen radical. In this experiment, the effect of light intensity was investigated at 40 and 82 W (due to instrumental limitation) and the results are shown in Figure 6. The results obtained in the investigation agree with above discussion. The reaction rate constant was observed to increase linearly with the increase in the light intensity for the investigated range.

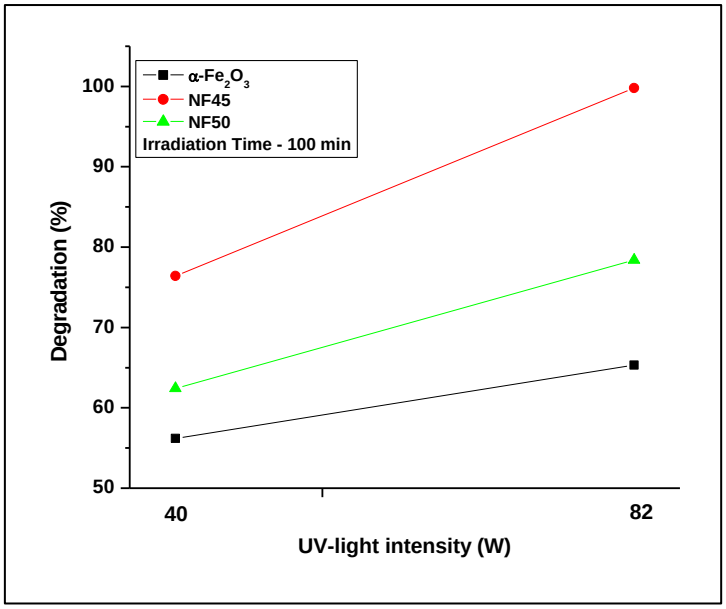

Figure 6: Effect of UV-light intensity on photodegradation of DB 199 dye

3.5.5 Effect of Addition of H_2O_2

The addition of hydroxyl radical producing species like H_2O_2 was regarded as a good parameter for enhancement of photocatalytic degradation process [31-33]. The results as shown in Figure 7, indicate that the hydrogen peroxide had accelerated the photocatalytic degradation of DB 199. The photocatalytic degradation rate of DB 199 increased when hydrogen peroxide concentration increased from 0 to 6 mol/l. The maximum degradation is achieved at H_2O_2 concentration of 4 mol/l. This could be due to the production of hydroxyl radical OH by photodissociation of H_2O_2 which is acting as strong oxidant and as electron scavengers [34].

$$H_2O_2 + e^- \xrightarrow{electron\ traping} OH^- + OH\bullet$$

It was assumed that, increasing the H_2O_2 concentration more than 4 mol/l, decreases the rate of photocatalytic degradation that could be due to by scavenging effect. However, High concentration of H_2O_2 inhibits catalytic activity as the molecules of H_2O_2 get adsorbed onto the catalyst surface instead of dissociating to form hydroxyl radicals.

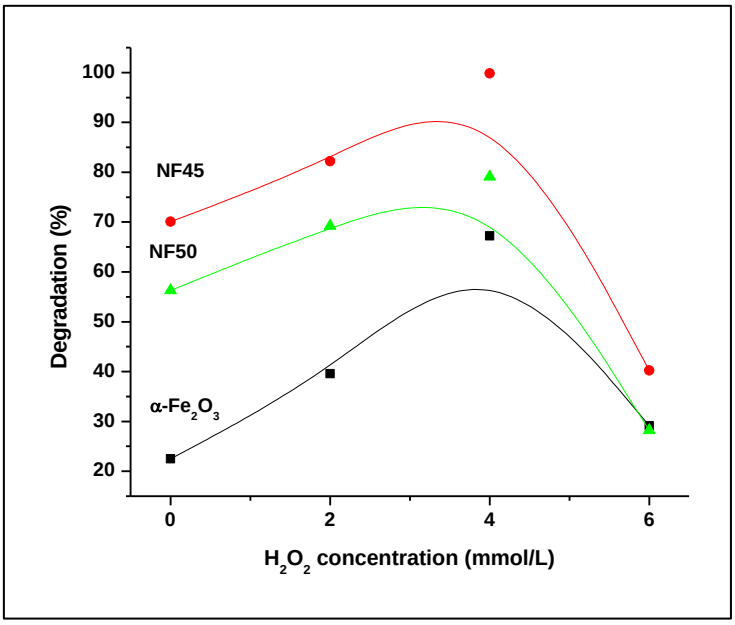

Figure 7. Effect of H_2O_2 addition on photodegradation of DB 199 dye

3.5.6 Stability test

In order to test the stability of the composite catalyst (20 mg/L), 10-times duplicate measurements were made with 100 min irradiation of DB 199 dye (100 ppm) at pH 3. The results are presented in Figure 8. From Figure 8, it can be observed that the degradation

efficiency of NF45 nanocomposite after the 7–times reuse was similar to the first time and start declining afterwards with remarkable change.

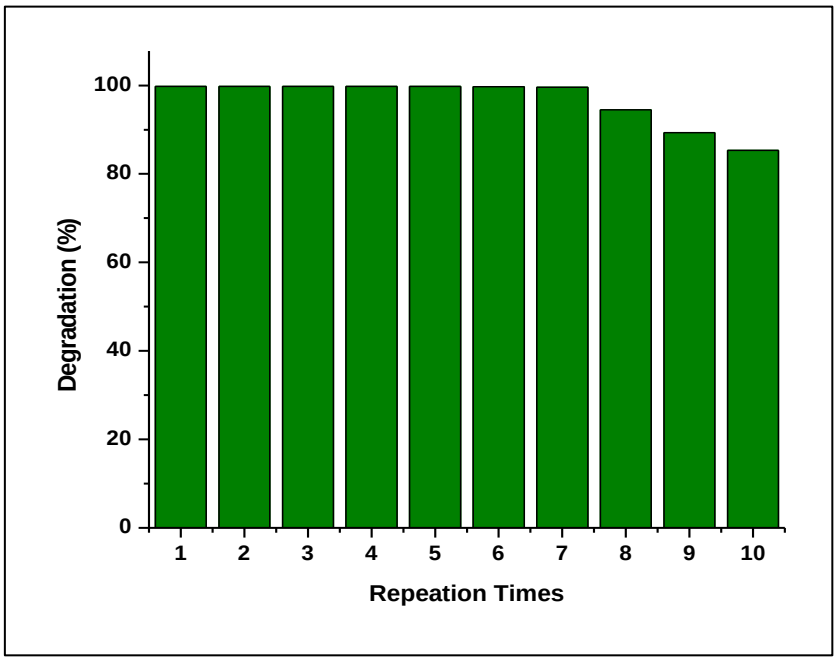

Figure 8: Experiment of repetitive use of NF45 nanocomposite

4. CONCLUSION

In this study, Nb_2O_5-α-Fe_2O_3 nanocomposites were synthesized by modified sol-gel method and photodegradation analysis of Direct Blue-199 (DB 199) dye was done following various photo-catalytic pathways. The calcination temperature was optimized to be 450°C and 550°C. The nanocomposite calcined at 450°C, was found to be the efficient material for photodegradation of DB 199 dye due to its large surface area (207.35 m^2/g) and smaller crystallite size 12.58 nm. Addition of H_2O_2 increases the decolorization rate, as it enhances the generation of •OH. But beyond a limit it has negative impact on the reaction rate. In stability test, as-synthesized sample showed steady photocatalytic efficiency for more than five times. Future work may be extended for degradation of the textile effluents containing dyes as major pollutants.

REFERENCES

1. Okpala, C. C. (2014). The benefits and applications of nanocomposites. *Int. J. Adv. Eng. Tech*, *12*, 18.
2. Kumar, A., Khan, M., He, J., & Lo, I. M. (2020). Visible–light–driven magnetically recyclable terephthalic acid functionalized g− C3N4/TiO2 heterojunction nanophotocatalyst for enhanced degradation of PPCPs. *Applied Catalysis B: Environmental*, *270*, 118898.
3. Hitam, C. N. C., & Jalil, A. A. (2020). A review on exploration of Fe2O3 photocatalyst towards degradation of dyes and organic contaminants. *Journal of environmental management*, *258*, 110050.
4. Huang, X., Hou, X., Song, F., Zhao, J., & Zhang, L. (2016). Facet-dependent Cr (VI) adsorption of hematite nanocrystals. *Environmental Science & Technology*, *50*(4), 1964-1972.
5. Huang, X., Zhao, Q., Young, R. P., Zhang, X., Walter, E. D., Chen, Y., ... & Rosso, K. M. (2020). Photo-production of reactive oxygen species and degradation of dissolved organic matter by hematite nanoplates functionalized by adsorbed oxalate. *Environmental Science: Nano*, *7*(8), 2278-2292.
6. Chen, C., Duan, F., Zhao, S., Wang, W., Yang, F., Nuansing, W., ... & Knez, M. (2019). Porous Fe2O3 nanotubes with α-γ phase junction for enhanced charge separation and photocatalytic property produced by molecular layer deposition. *Applied Catalysis B: Environmental*, *248*, 218-225.
7. Huang, X., Hou, X., Jia, F., Song, F., Zhao, J., & Zhang, L. (2017). Ascorbate-promoted surface iron cycle for efficient heterogeneous Fenton alachlor degradation with hematite nanocrystals. *ACS Applied Materials & Interfaces*, *9*(10), 8751-8758.
8. Mishra, M., & Chun, D. M. (2015). α-Fe2O3 as a photocatalytic material: A review. *Applied Catalysis A: General*, *498*, 126-141.
9. Luo, N., Montini, T., Zhang, J., Fornasiero, P., Fonda, E., Hou, T., ... & Wang, F. (2019). Visible-light-driven coproduction of diesel precursors and hydrogen from lignocellulose-derived methylfurans. *Nature Energy*, *4*(7), 575-584.
10. Ghaffari, Y., Gupta, N. K., Bae, J., & Kim, K. S. (2020). One-step fabrication of Fe2O3/Mn2O3 nanocomposite for rapid photodegradation of

organic dyes at neutral pH. *Journal of Molecular Liquids*, *315*, 113691.
11. Bilgic, A. (2022). Fabrication of monoBODIPY-functionalized Fe3O4@ SiO2@ TiO2 nanoparticles for the photocatalytic degradation of rhodamine B under UV irradiation and the detection and removal of Cu (II) ions in aqueous solutions. *Journal of Alloys and Compounds*, *899*, 163360.
12. Kim, S., Gupta, N. K., Bae, J., & Kim, K. S. (2021). Fabrication of coral-like Mn2O3/Fe2O3 nanocomposite for room temperature removal of hydrogen sulfide. *Journal of Environmental Chemical Engineering*, *9*(3), 105216.
13. Liu, H., Li, H., Lu, J., Zeng, S., Wang, M., Luo, N., ... & Wang, F. (2018). Photocatalytic cleavage of C–C bond in lignin models under visible light on mesoporous graphitic carbon nitride through π–π stacking interaction. *ACS Catalysis*, *8*(6), 4761-4771.
14. Su, T., Shao, Q., Qin, Z., Guo, Z., & Wu, Z. (2018). Role of interfaces in two-dimensional photocatalyst for water splitting. *Acs Catalysis*, *8*(3), 2253-2276.
15. Kampouri, S., Nguyen, T. N., Spodaryk, M., Palgrave, R. G., Züttel, A., Smit, B., & Stylianou, K. C. (2018). Concurrent photocatalytic hydrogen generation and dye degradation using MIL-125-NH2 under visible light irradiation. *Advanced Functional Materials*, *28*(52), 1806368.
16. Melchionna, M., & Fornasiero, P. (2020). Updates on the Roadmap for Photocatalysis. *Acs Catalysis*, *10*(10), 5493-5501.
17. Daâssi, D., Rodríguez-Couto, S., Nasri, M., & Mechichi, T. (2014). Biodegradation of textile dyes by immobilized laccase from Coriolopsis gallica into Ca-alginate beads. *International Biodeterioration & Biodegradation*, *90*, 71-78.
18. Adegoke, K. A., & Bello, O. S. (2015). Dye sequestration using agricultural wastes as adsorbents. *Water resources and industry*, *12*, 8-24.
19. El Harfi, S., & El Harfi, A. (2017). Classifications, properties and applications of textile dyes: A review. *Applied Journal of Environmental Engineering Science*, *3*(3), 00000J-Envir.
20. Shivaraju, H. P., Midhun, G., Anil Kumar, K. M., Pallavi, S., Pallavi, N., & Behzad, S. (2017). Degradation of selected industrial dyes using Mg-doped TiO 2 polyscales under natural sun light as an alternative driving energy. *Applied Water Science*, *7*, 3937-3948.
21. Katheresan, V., Kansedo, J., & Lau, S. Y. (2018). Efficiency of various recent wastewater dye removal methods: A review. *Journal of environmental chemical engineering*, *6*(4), 4676-4697.
22. Li, X., Wei, W., Wang, S., Kuai, L., & Geng, B. (2011). Single-crystalline α-Fe2O3 oblique nanoparallelepipeds: High-yield synthesis, growth mechanism and structure enhanced gas-sensing properties. *Nanoscale*, *3*(2), 718-724.
23. Hashimoto, T., Yamada, T., & Yoko, T. (1996). Third-order nonlinear optical properties of sol–gel derived α-Fe2O3, γ-Fe2O3, and Fe3O4 thin films. *Journal of applied physics*, *80*(6), 3184-3190.
24. Ingler Jr, W. B., & Khan, S. U. (2005). Photoresponse of spray pyrolytically synthesized copper-doped p-Fe2O3 thin film electrodes in water splitting. *International Journal of Hydrogen Energy*, *30*(8), 821-827.
25. Zhao, H., Xu, S., Zhong, J., & Bao, X. (2004). Kinetic study on the photo-catalytic degradation of pyridine in TiO2 suspension systems. *Catalysis Today*, *93*, 857-861.
26. Qourzal, S., Tamimi, M., Assabbane, A., & Ait-Ichou, Y. (2005). Photocatalytic degradation and adsorption of 2-naphthol on suspended TiO2 surface in a dynamic reactor. *Journal of Colloid and Interface Science*, *286*(2), 621-626.
27. Kansal, S. K., Kaur, N., & Singh, S. (2009). Photocatalytic degradation of two commercial reactive dyes in aqueous phase using nanophotocatalysts. *Nanoscale research letters*, *4*, 709-716.
28. Rauf, M. A., & Ashraf, S. S. (2009). Fundamental principles and application of heterogeneous photocatalytic degradation of dyes in solution. *Chemical engineering journal*, *151*(1-3), 10-18.
29. Watts, M. J., & Cooper, A. T. (2008). Photocatalysis of 4-chlorophenol mediated by TiO2 fixed to concrete surfaces. *Solar Energy*, *82*(3), 206-211.
30. Ajmal, A., Majeed, I., Malik, R. N., Idriss, H., & Nadeem, M. A. (2014). Principles and mechanisms of photocatalytic dye degradation on TiO 2 based photocatalysts: a comparative overview. *Rsc Advances*, *4*(70), 37003-37026.
31. Qourzal, S., Tamimi, M., Assabbane, A., & Ait-Ichou, Y. (2007). TiO2 photocatalytic mineralization of beta-naphthol: Influence of some inorganic ions, ethanol, and hydrogen peroxide. *Comptes Rendus Chimie*, *10*(12), 1187-1194.
32. Touati, A., Hammedi, T., Najjar, W., Ksibi, Z., & Sayadi, S. (2016). Photocatalytic degradation of textile wastewater in presence of hydrogen peroxide: Effect of cerium doping titania. *Journal of Industrial and Engineering Chemistry*, *35*, 36-44.
33. Tseng, D. H., Juang, L. C., & Huang, H. H. (2012). Effect of oxygen and hydrogen peroxide on the photocatalytic degradation of monochlorobenzene in TiO2 aqueous suspension. *International Journal of Photoenergy*, *2012*(1), 328526.
34. Muruganandham, M., Sobana, N., & Swaminathan, M. (2006). Solar assisted photocatalytic and photochemical degradation of Reactive Black 5. *Journal of hazardous materials*, *137*(3), 1371-1376.

Cite This Article: M.J. Pawar, A.D. Khajone, M.D. Gaonar (2024). Photocatalytic activity of Nb2O5-α-Fe2O3 Nanocomposites Synthesized by Sol-gel Method. *East African Scholars Multidiscip Bull*, *7*(5), 71-78.